nature portfolio

https://doi.org/10.1038/s41557-021-00850-8

Supplementary information

A photosensitizer–polyoxometalate dyad that enables the decoupling of light and dark reactions for delayed on-demand solar hydrogen production

In the format provided by the authors and unedited

Supplementary Information

A photosensitiser-polyoxometalate dyad that enables the decoupling of light- and dark-reactions for delayed on-demand solar hydrogen production

Sebastian Amthor,[a] Sebastian Knoll,[a] Magdalena Heiland,[a] Linda Zedler,[b] Chunyu Li,[c] Djawed Nauroozi,[a] Willi Tobaschus,[d,e,f] Alexander K. Mengele,[a] Montaha Anjass,[a,g] Ulrich S. Schubert,[d,e,f] Benjamin Dietzek,[b,c,f]* Sven Rau,[a]* and Carsten Streb[a,g]*

a Ulm University, Institute of Inorganic Chemistry I, Albert-Einstein-Allee 11, 89081 Ulm, Germany, e-mail: sven.rau@uni-ulm.de; carsten.streb@uni-ulm.de

b Department Functional Interfaces, Leibniz Institute of Photonic Technology Jena (IPHT), Albert-Einstein-Straße 9, 07745 Jena, Germany, e-mail: benjamin.dietzek@leibniz-ipht.de

c Institute of Physical Chemistry, Friedrich Schiller University Jena, Helmholtzweg 4, 07743 Jena, Germany, e-mail: benjamin.dietzek@uni-jena.de

d Laboratory of Organic and Macromolecular Chemistry (IOMC), Friedrich Schiller University Jena, Humboldstr. 10, 07743 Jena, Germany

e Jena Center of Soft Matter (JCSM), Friedrich Schiller University Jena, Philosophenweg 7, 07743 Jena, Germany

f Center for Energy and Environmental Chemistry Jena (CEEC Jena), Friedrich Schiller University Jena, Philosophenweg 7a, 07743 Jena, Germany

g Helmholtz-Institute Ulm (HIU), Helmholtzstr. 11, 89081 Ulm, Germany

Table of contents

1. Methods and Materials

Materials: 4,4'-dimethyl-2,2'-bipyridine was purchased from ABCR. The synthesis of $[(tbbpy)_2RuCl_2]$[1] and $K_{10}[\alpha\text{-}P_2W_{17}O_{61}]\times 17H_2O$[2] are literature-known. All solvents used (except for deuterated solvents) were water-free if not stated otherwise.

NMR spectroscopy: ^1H (400.13 MHz) and ^{31}P (161.98 MHz) NMR spectra were recorded with a Bruker DRX 400 spectrometer. The NMR spectra were recorded in CD_3CN, $CDCl_3$ or $(CD_3)_2SO$ at 298 K. ^1H-NMR chemical shifts were referenced to the solvent peak for acetonitrile (δ = 1.94 ppm), chloroform (δ = 7.260 ppm) or dimethyl sulfoxide (δ = 2.500 ppm). NMR spectroscopic data was analyzed using MestReNova V6.0.2-5475.

Mass spectrometry (MS): MS analysis was performed on a Bruker solariX (2010) Hybrid 7 TFT-ICR for MALDI and with a Bruker Ultraflex III MALDI TOF/TOF for MALDI/TOF measurements. Mass data was converted using Compass DataAnalysisViewer V5.0.

UV-Vis-NIR absorption spectroscopy: UV-vis-NIR spectra were recorded on a JASCO spectrometer V-670. Steady-state UV-Vis spectra were recorded on a single-channel fiber-optic spectrometer (Avantes AvaSpec-ULS2048XL) using a deuterium-halogen light source (Avantes AvaLight DH-S-BAL). Time-dependent UV-vis spectra were recorded on a single-channel SPECORD S 600 (AnalytikJena). Quartz cells with a 10 mm path length were used.

Thermogravimetric analysis (TGA): TGA was performed on a Netzsch TG 209 F1 Libra thermobalance at a heating rate of 5 K min^{-1} in air.

Emission spectroscopy: steady-state emission spectra were recorded on a JASCO 25 spectro-fluorometer FP-8500. Quartz cells with a 10 mm path length were used. Samples were cross-validated using UV-Vis-NIR spectroscopy to ensure identical absorbances at 450nm.

ATR-IR spectroscopy: ATR-IR experiments were performed on a Bruker Alpha II spectrometer equipped with a diamond ATR cell.

Electrochemical characterization: electrochemical measurements were performed using an Autolab potentiostat PGSTAT204 (Metrohm) in three-electrode configuration. Working electrode: glassy carbon disc, diameter 3 mm; counter-electrode: Pt wire; reference electrode: non-aqueous Ag/Ag^+ electrode with 0.01 M $AgNO_3$ in acetonitrile. The ferrocenium/ferrocene (Fc^+/Fc) redox couple was used as internal reference.

Spectro-electrochemical (SEC) characterization: Time-dependent UV-Vis absorption spectra during photochemical-, chemical- or electrochemical reactions were recorded with an Avantes AvaSpec-ULS2048CL-EVO-(CMOS) spectrophotometer connected to an Avantes AvaLight-DH-S-BAL light source via fiber-optic cables (Data acquisition time usually 1.5 ms and averaged over 100 measurements). UV-Vis spectroelectrochemical measurements at room temperature were conducted with a commercial honeycomb thin-layer spectroelectrochemistry cell from Pine Research Instrumentation, employing a screen-printed platinum working and counter electrode and a Ag/Ag^+ (0.01 M $AgNO_3$ in acetonitrile) reference electrode. The effective path length is 1.7 mm. Constant cell potentials were applied during the spectroelectrochemistry measurements using an Autolab potentiostat PGSTAT204 (Metrohm).

Resonance Raman (rR) spectroscopy and spectro-electrochemistry: For rR spectroscopy, visible diode lasers at 405 (TopMode-405-HP, Toptica, Germany), 473 (HB-Laser, Germany), 532 (HB-Laser, Germany) and 643 nm (CrystaLaser, USA) have been used

for excitation. For spectral detection, an IsoPlane 160 spectrometer (Princeton Instruments, USA) has been used applying an entrance slit width of 50 µm and diffraction gratings with either 2400 or 1200 grooves/mm. The laser power has been attenuated to approximately 5 mW to reduce photodegradation of the analyte. The Raman scattered signals were collected in transmission and filtered from laser light using dielectric long pass filters (Semrock, USA) before being focused onto the spectrograph's entrance slit. The spectrally dispersed Raman scattered photons were detected by a thermoelectrically cooled CCD camera of 1340 x 100 pixels (PIXIS eXcelon, Princeton Instruments, USA). The band of DMF at 1407 cm^{-1} was used as a reference for normalizing Raman intensities and calibration of the wavenumber scale. Spectral post processing includes background correction, normalization, and subtraction of the solvent spectrum. UV-Vis-, rR-SEC and electrochemical measurements shown in Fig. S24 were performed as described previously.[3] Briefly, all spectroelectrochemical measurements were performed in a fused silica cuvette of 1 mm pathlength (Hellma, Bioanalytical Systems, USA) employing a three-electrode configuration consisting of a Pt counter electrode, an Ag/AgCl pseudo-reference electrode and a glassy carbon working electrode. Potential-controlled monitoring of spectral changes as well as cyclic voltammetry have been carried out using a computer-controlled VersaSTAT 3 potentiostat (Princeton Applied Research, USA).

Transient absorption spectroscopy: Femtosecond transient absorption (fs-TA) data were recorded using a custom-built optical setup, as previously described in detail.[4] For excitation, a 1 kHz-pulse repetition rate Ti:Sapphire regenerative amplifier (Libra, Coherent, USA) has been used. A fraction of the laser output is focused into a CaF_2 plate mounted on a rotating stage for generating the white-light supercontinuum pulse. This broad band pulse is split in reference and probe pulse. The other part of the laser output is used to generate the pump pulse of roughly 100 fs pulse duration by SHG generation of the fundamental in a nonlinear crystal (400 nm). A mechanical chopper is used to reduce the repetition rate of the pump pulses to 0.5 kHz and the mutual polarization of pump and probe pulses is adjusted to the magic angle of 54.7° by a Berek compensator and a polarizer. The probe pulse is focused into the 1mm-cuvette using a 500 mm focal length concave mirror. The spectra of probe and reference pulses are detected by a Czerny-Turner spectrograph of 150 mm focal length (SP2150, Princeton Instruments) equipped with a diode array detector (Pascher Instruments AB, Sweden). During ca. 300 fs around time zero strong contributions from coherent artifact signals[5] are observed, which inhibit analyzing the pump-probe data by multi-exponential fitting algorithms at shorter time delay. Data analysis includes first a spectral preprocessing step for chirp correction before a sum of exponential functions is fitted to the data by least squares regression analysis using custom software (Pascher Instruments AB, Lund, Sweden). The pulse overlap region of ±150 fs is removed from the data analysis due to coherent artefacts mentioned above. The amplitudes of the exponential fit correspond to the decay associated spectra (DAS). For the investigation of the primary photoinduced processes, the sample was dissolved in anhydrous DMF (OD (400 nm) = 0.3 in a cell with 1 mm path length).

Nanosecond transient emission spectroscopy: Nanosecond transient emission spectroscopy was used to study the lifetime of the long-lived species. The pump pulses centered at 355 nm were produced by a continuum surelite Nd:YAG laser system (pulse duration 5 ns, repetition rate 10 Hz). A Continuum OPO Plus pumped by a Continuum Surelite Nd:YAG laser generated the pump pulses at 470 nm. The power of the pump beam was kept at 0.2 mJ per pulse. The probe light is provided by a 75 W xenon arc lamp. Spherical concave mirrors are used to focus the probe beam into the samples and then to send the beam to the monochromator (Acton, Princeton Instruments). The spectrally selected probe light is detected by a Hamamatsu R928 photomultiplier. Time-resolved emission spectra were recorded by

using a 475 nm long pass filter before the detector to eliminate the pump scattering. The signal is amplified and processed by a commercially available detection system (Pascher Instruments AB). Each sample was freshly prepared and its optical density was kept at *ca.* 0.2 at the excitation wavelength. All measurements were performed in 1 cm path length fluorescence cuvettes.

The stability of the samples during all spectroscopic experiments was checked by measuring absorption spectra before and after each spectroscopic run.

Gas-chromatography (GC): Gas-chromatography was performed on a Bruker Scion GC/MS, with a thermal conductivity detector 15 (column: molecular sieve 5A, *l* = 75 m, *d* = 0.53 mm, oven temperature 70 °C, flow rate 30 mL min^{-1}, detector temperature 200 °C) with Argon as the carrier gas. The GC was calibrated by direct injection of known amounts of H_2 gas.

Single-crystal X-ray diffraction (sc-XRD): Single crystals suitable for X-ray crystallography were mounted using a MicroLoop and perfluoropolyalkyl ether. X-ray diffraction intensity data were measured at 150 K on a Bruker D8 Quest single crystal diffractometer with a PHOTON II detector using Mo-Kα radiation (wavelength λ = 0.71073 Å). Structure solution and refinement were carried out using the SHELXL package[6,7] *via* Olex2. Corrections for incident and diffracted beam absorption effects were applied using multi-scan refinements. Structures were solved by direct methods and refined against F^2 by the full-matrix least-squares technique. The hydrogen atoms were included at calculated positions with fixed thermal parameters. All non-hydrogen atoms were refined anisotropically unless stated otherwise. Mercury was used for graphical representation.[8]

Quantum yield determination: Quantum yields were determined using a custom-built, literature reported setup[9] measuring the light power (P_{sample}, eq. 1, detector: PowerMax USB – PS19Q Coherent) of a monochromatic LED (λ_{max} = 470 nm, OSRAM LBCP7P-GYHY powered by a Basetech BT-153 0 – 15V/DC 0- 3 A 45 W) focused (Nikkor AF 50/1,4D) on the sample cuvette (quartz glass, optical path length 1.0 cm).

Photostability: Photostability experiments (main manuscript, Figure 3) were conducted in water-free, de-aerated DMF at the following concentrations: [**PS-POM**] = 2.9 µM, [**1**] = 5.8 µM. The samples were irradiated using a 470 nm LED, *P ca.* 40-50 mW/cm^2 integrated into a custom reactor cooled by four fans, to control room temperature during irradiation.

2. Synthesis and Characterization

4-(PO_3Et_2)-4'-methyl-2,2'-bipyridine ((mPO_3Et_2)bpy) was synthesized using a literature known procedure, giving the target product in yields of 24% (based on the precursor 4,4'-dimethyl-2,2'-bipyridine).[10] Crystals suitable for X-ray diffraction were obtained by slow evaporation of a chloroform solution of (mPO_3Et_2)bpy, see Section 9.

^{1}H NMR (400 MHz, $CDCl_3$) *δ* 8.65 (d, *J* = 5.1 Hz, 1H), 8.61 (dd, *J* = 5.1, 0.5 Hz, 1H), 8.36 (m, 1H), 8.27 (dt, J = 1.5, 0.7 Hz, 1H), 7.40 – 7.34 (m, 1H), 7.24 (ddd, *J* = 5.1, 1.7, 0.7 Hz, 1H), 4.19 – 3.94 (m, 4H), 3.26 (d, *J* = 22.3 Hz, 2H), 2.48 (s, 3H), 1.41 – 1.15 (m, 6H).

^{31}P NMR (162 MHz, $CDCl_3$) *δ* 25.02.

[($tbbpy)_2$Ru(mPO_3Et_2)bpy](PF_6)$_2$ (1): (mPO_3Et_2)bpy (0.69 g, 2.15 mmol) and [($tbbpy)_2RuCl_2$] (1.0 g, 1.41 mmol) were added to an ethanol water mixture (3 : 1, v/v, 40 mL) and heated under reflux for 24 h. Then, the ethanol was evaporated in vacuum and an excess of ammonium

hexafluorophosphate (28 mmol, 4.5 g) was added to the resulting aqueous solution. The resulting precipitate was filtered off and was subsequently purified using size exclusion chromatography (Sephadex LH-20, methanol) yielding a deep red powder (1.7 g, 97% based on $[(tbbpy)_2RuCl_2]$).

^{1}H NMR (400 MHz, CD_3CN) δ 8.54 – 8.45 (m, 4H), 8.43 – 8.39 (m, 1H), 8.37-8.34 (m, 1H), 7.64 – 7.56 (m, 5H), 7.52 (d, *J* = 5.8 Hz, 1H), 7.44 – 7.37 (m, 4H), 7.37 – 7.33 (m, 1H), 7.30 – 7.24 (m, 1H), 4.03 (dqd, *J* = 8.5, 7.1, 3.4 Hz, 4H), 3.39 (d, *J* = 22.5 Hz, 2H), 2.52 (s, 3H), 1.44 – 1.41 (m, 36H), 1.17 (td, *J* = 7.0, 1.5 Hz, 6H).

^{31}P NMR (162 MHz, CD_3CN) δ 22.81.

HR-MALDI-MS m/z (calc. for $C_{52}H_{69}F_6N_6O_3P_2Ru$) 1103.38541; m/z (observed for $[M\text{-}PF_6]^+$) 1103.38473.

$(n$Bu$_4$N)$_7$K$_3$[α$_2$-P$_2$W$_{17}$O$_{61}$] (1): 10 g (2.19 mmol) $K_{10}[\alpha_2\text{-}P_2W_{17}O_{61}]\cdot 17\ H_2O$ were dissolved in 200 mL water at 95 °C. 35.0 g (108 mmol) solid nBu$_4$NCl was added. The resulting suspension was stirred for 15 min at 95 °C and filtered. The white solid was washed with 250 mL H_2O and dried for one day in air. Yield: 10.0 g (75 % based on $K_{10}[\alpha_2\text{-}P_2W_{17}O_{61}]\cdot 17\ H_2O$).

ATR-FT-IR ($\tilde{\nu}$ [cm^{-1}]): 422, 469, 485, 526, 565, 598, 624, 731, 771, 813, 882, 915, 934, 952, 987, 1016, 1030, 1056, 1080, 1152, 1378, 1464, 1483, 1630, 1643, 2870, 2932, 2959.

^{1}H NMR (400 MHz, Acetone) δ 3.62 – 3.44 (m, 8H), 1.91 – 1.69 (m, 8H), 1.62 – 1.44 (m, 8H), 0.99 (t, J = 7.3 Hz, 12H).

^{31}P NMR (162 MHz, Acetone) δ -9.04, -13.38.

$(n$Bu$_4$N)K[P$_2$W$_{17}$O$_{61}${((mPO$_3$)bpy)Ru(tbbpy)$_2$}$_2$] (PS-POM): 1 (0.285 g, 0.23 mmol, 2.8 eq.) was dissolved in de-aerated dichloromethane (10 mL) in a glovebox and trimethylsilyl bromide (TMSBr) (130 µL, 0.91 mmol, 4 eq.) was added to the solution (resulting in the formation **1a**, *i.e.* TMS-functionalized **1**, see main manuscript Fig. 2a). The mixture was stirred for 12 h at r.t. Then, the solvent and excess TMSBr were removed under reduced pressure. The residue was taken up in a small amount of dichloromethane (~5 mL) and filtered through a frit (porosity 4). The obtained solution was diluted to a volume of 10 mL with dichloromethane and stirred for 5 min at r.t. $(n\text{Bu}_4\text{N})_7\text{K}_3[\alpha\text{-}P_2W_{17}O_{61}]$ (0.480 g, 0,08 mmol, 1 eq.) was added as a solid to the solution. Upon addition the solution decolorizes immediately. The suspension was further stirred for 12 h at r.t. After that time the solid was filtered off and washed with dichloromethane until the filtrate was clear. The crude product was purified by slow diffusion of dichloromethane (DCM) into a DMF (50 mL) solution giving an orange-red powder. The powder was recovered by centrifugation and washed with DCM, then dissolved in 5 mL DMF. To the solution, 1.5 g nBu$_4$NCl (5.4 mmol) were added. To this, water (25 ml) was added, resulting in an orange precipitate. The precipitate was washed with a water/ethanol solution (30 mL/5 mL), ethanol (2 x 25 mL) and diethyl ether (2 x 25 mL). The precipitate was re-dissolved in DMF (50 mL). Slow diffusion of DCM into this solution gave an orange-red powder, which was recovered by filtration, washed with diethyl ether, and dried to give pure **PS-POM**. Yield: 280 mg (0.045 mmol), 57% based on $(n\text{Bu}_4\text{N})_7\text{K}_3[\alpha_2\text{-}P_2W_{17}O_{61}]$).

^{1}H NMR (400 MHz, DMSO) δ 8.77 (dd, *J* = 16.7, 14.0 Hz, 10H), 8.47 (d, *J* = 4.5 Hz, 2H), 7.71 – 7.47 (m, 22H), 7.40 (dd, *J* = 10.3, 4.4 Hz, 2H), 1.51 – 1.62 (m, 6H), 1.44 – 1.34 (m, 72H).

^{31}P NMR (162 MHz, DMSO) δ 20.14, 20.01, -11.26, -12.70.

MALDI-TOF (Peptide Mix, negative-ion mode): m/z calc. $C_{112}H_{156}N_{13}O_{64}P_4Ru_2W_{17}$ 3080; m/z observed: 3080 [M - (K^+) - ($n$$Bu_4N^+$) + ($H_2O$)]$^{2-}$.

O,O-dimethyl-benzyl phosphonate: 1.62 g (9.5 mmol) benzyl bromide and 6 mL (49 mmol) $P(OMe)_3$ were mixed and refluxed at 110 °C for 24 h. The $P(OMe)_3$ was distilled off in vacuum (50 °C / $1 \cdot 10^{-3}$ mbar). The final product was obtained as a colourless oil. Yield: 1.9 g (9.5mmol / 100% based on benzyl bromide).

^{1}H NMR (400 MHz, MeOD) δ 7.35 – 7.28 (m, 4H), 7.28 – 7.21 (m, 1H), 3.67 (d, J = 10.9 Hz, 6H), 3.25 (d, J = 21.8 Hz, 2H).

^{13}C NMR (101 MHz, MeOD) δ 132.48, 132.38, 130.96, 130.89, 129.62, 129.59, 128.09, 128.05, 53.64, 53.57, 33.31, 31.95.

^{31}P NMR (162 MHz, MeOD) δ 30.20.

($n$$Bu_4N)_5K[\alpha_2$-$P_2W_{17}O_{61}(POCH_2C_6H_5)]$ (Bz-POM): 0.50 g (0.084 mmol) of ($n$$Bu_4N)_7K_3[\alpha_2$-$P_2W_{17}O_{61}$] (**1**), 0.05 g (0.28 mmol) *O,O*-dimethyl-benzyl phosphonate and 0.43 g (4.4 mmol) tetra-*n*-butylammonium chloride were dissolved in 18 mL *N*,*N*-dimethyl acetamide. 0.6 mL of 12 M aqueous HCl were added and the resulting solution was heated at 110 °C for 1 h in the microwave. After cooling to room temperature, the product was precipitated with 100 mL diethyl ether, washed twice with 50 mL ethanol and twice with 50 mL diethyl ether. The crude, yellowish product was redissolved in 50 mL acetonitrile: water (6:1) and precipitated by addition of 2.00 g (6.2 mmol) tetra-*n*-butylammonium bromide. The yellow precipitate was washed twice with 25 mL water, twice with 10 mL ethanol and twice with 10 mL diethyl ether. The yellow product was air-dried for one day, yielding 0.4 g (0.070 mmol / 83% based on **1**).

^{1}H NMR (400 MHz, DMSO) δ 7.37 (dt, J = 7.6, 2.0 Hz, 4H), 7.22 (t, J = 7.4 Hz, 4H), 7.16 (dt, J = 8.3, 3.9 Hz, 2H), 3.23 – 3.11 (m, 40H), 1.67 – 1.47 (m, 40H), 1.32 (h, J = 7.4 Hz, 40H), 0.94 (t, J = 7.3 Hz, 60H).

^{31}P NMR (162 MHz, DMSO) δ 23.14, -11.37, -12.97.

ATR-FT-IR ($\tilde{\nu}$ [cm^{-1}]): 2960, 2933, 2874, 1484, 1464, 1457, 1379, 1269, 1194, 1163, 1153, 1120, 1089, 1052, 1041, 1021, 994, 972, 955, 943, 813, 780, 735, 698, 620, 597, 585, 568, 537, 531, 482, 471, 455, 422.

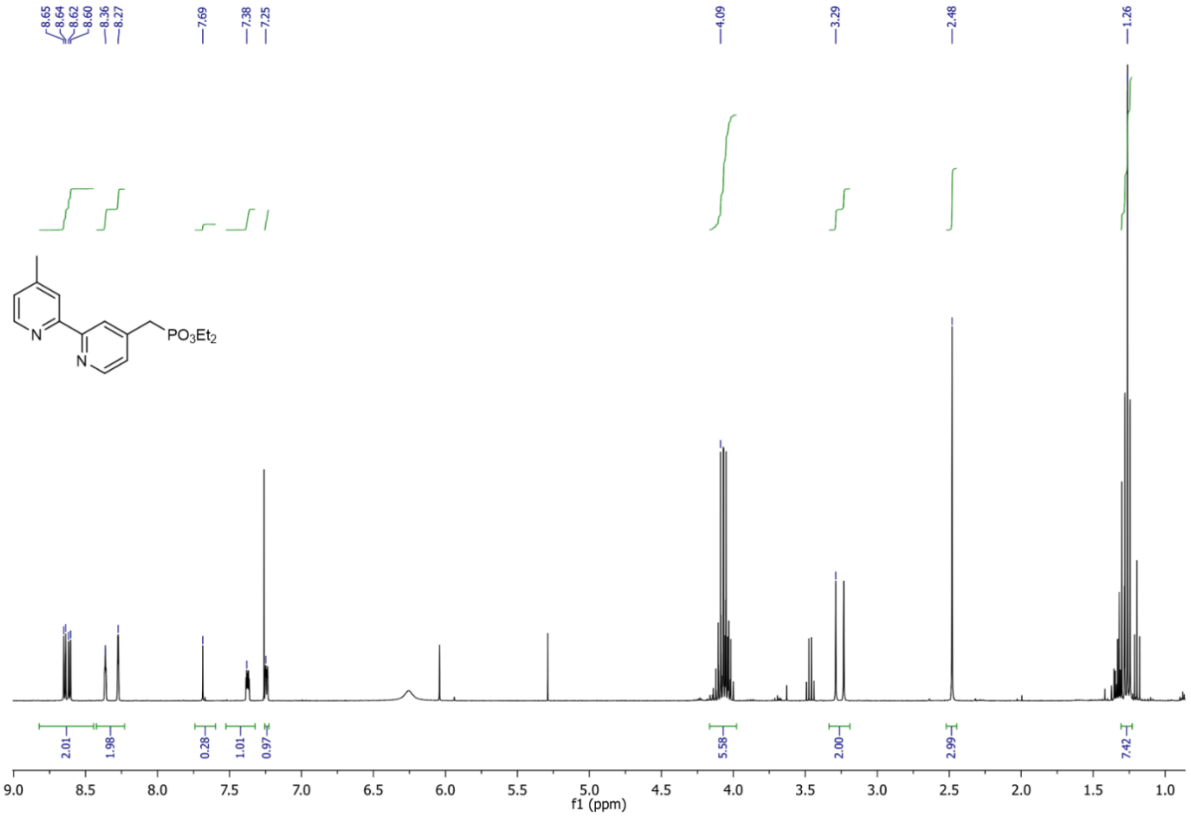

Figure 1: ^{1}H-NMR spectrum of (mPO_3Et_2)bpy in $CDCl_3$ at r.t..

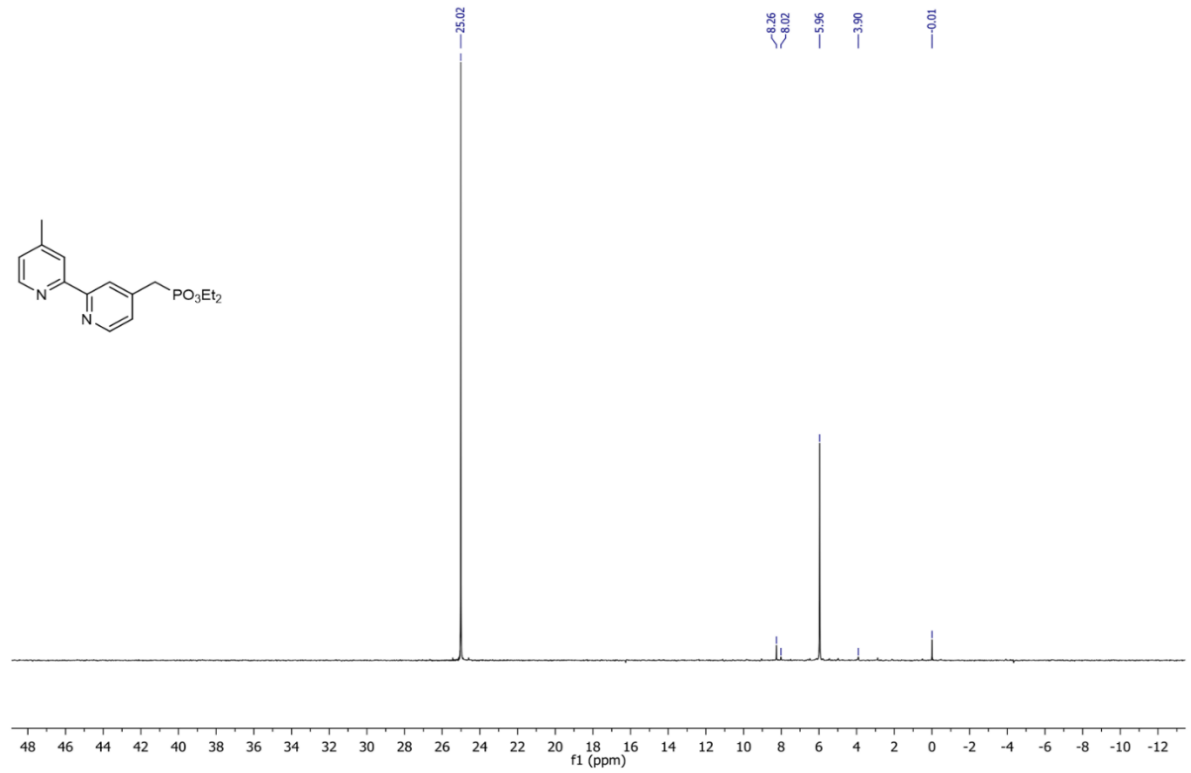

Figure 2: ^{31}P-NMR spectrum of (mPO_3Et_2)bpy in $CDCl_3$ at r.t.

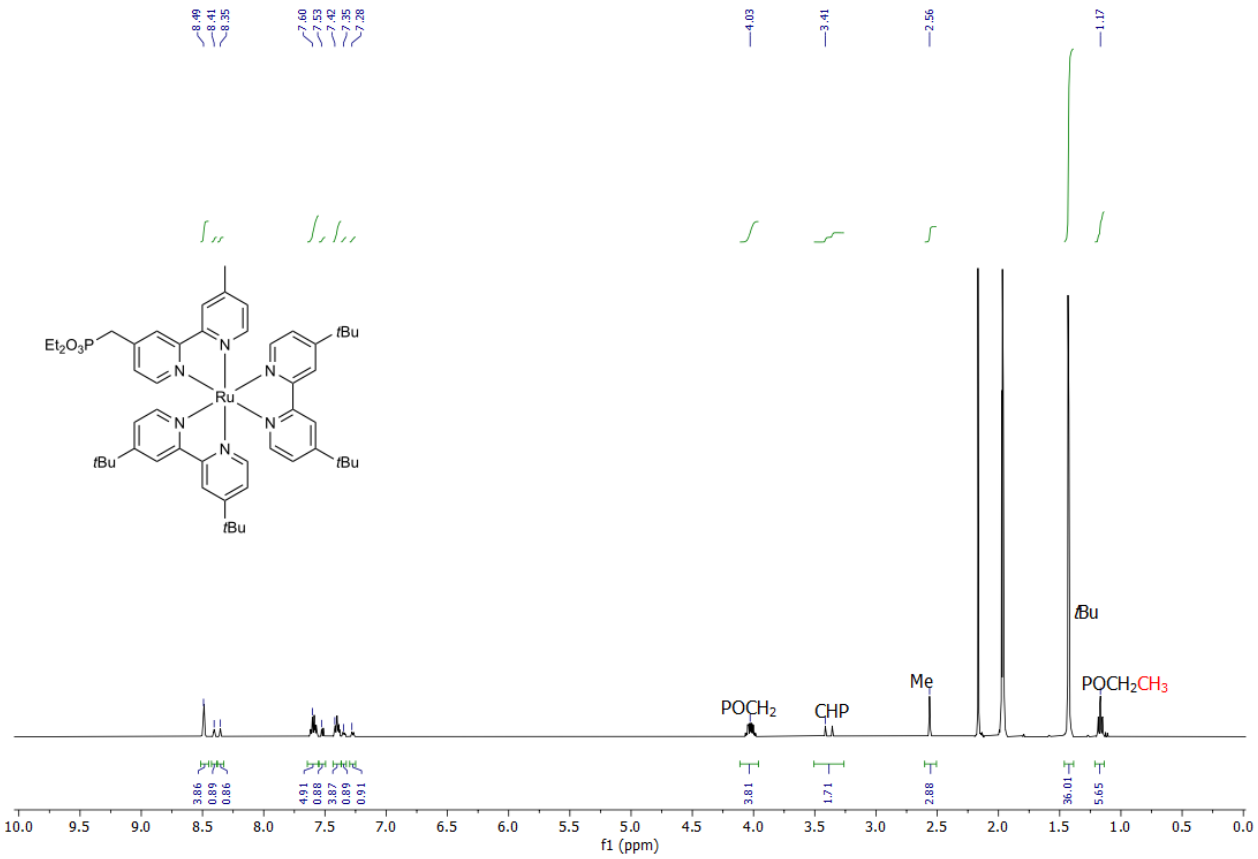

Figure 3: ^{1}H-NMR spectrum of **1** in acetonitrile-d_3 at r.t.

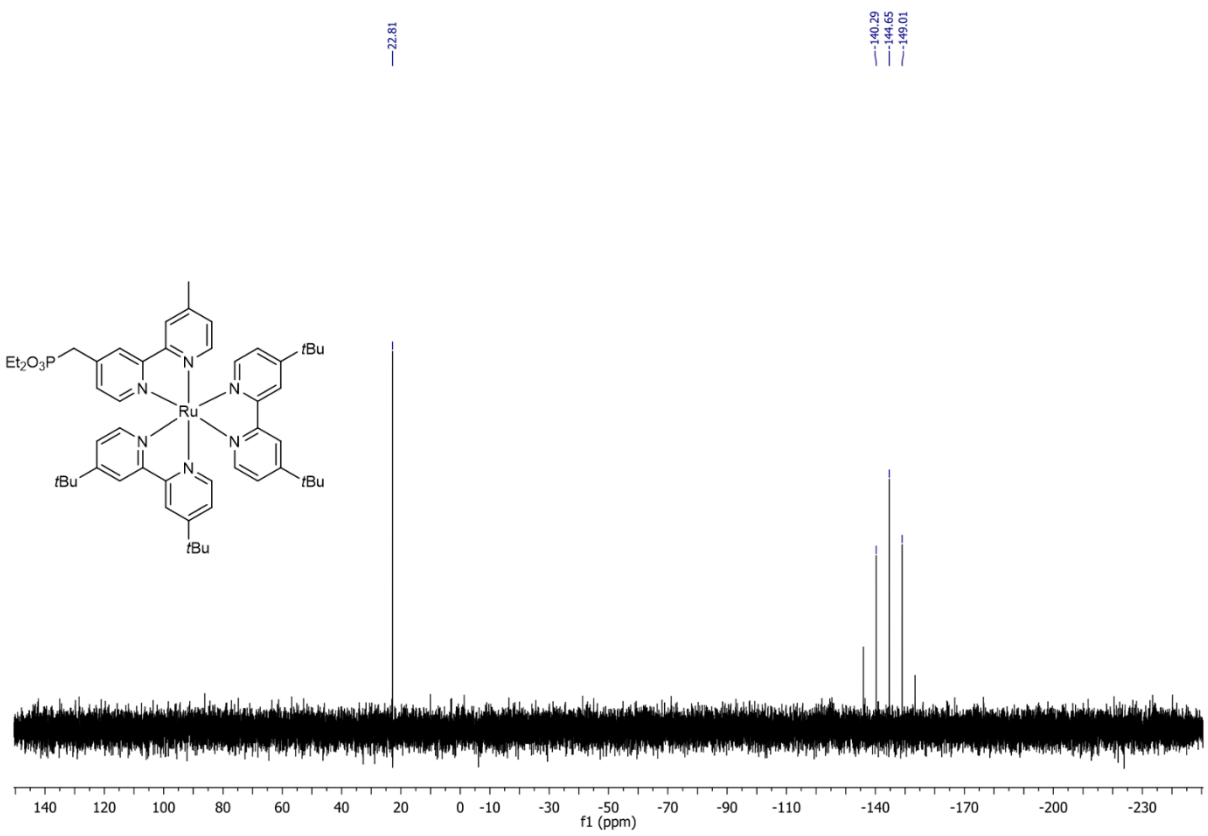

Figure 4: ^{31}P-NMR spectrum of **1** in acetonitrile-d_3 at r.t.

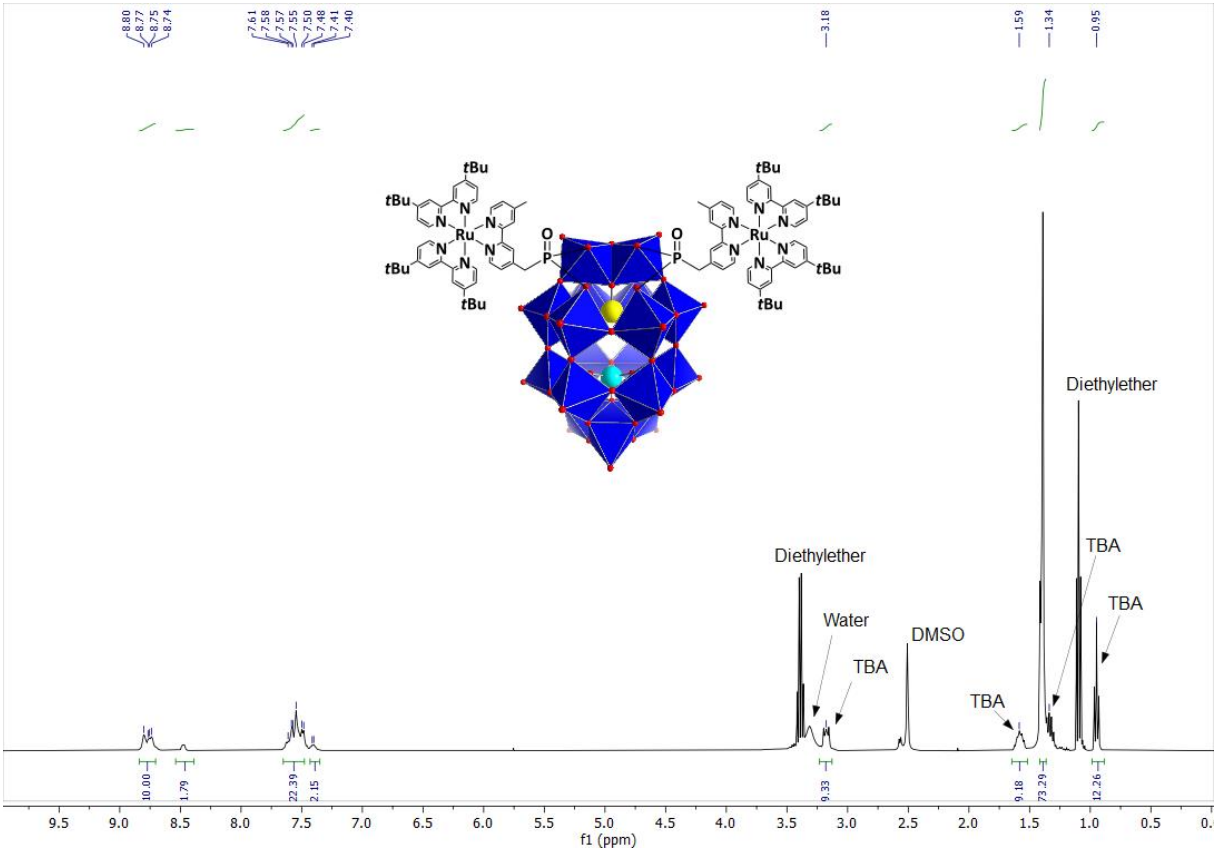

Figure 5: ^{1}H-NMR of **PS-POM** in DMSO-d_6 at r.t. DMSO: dimethyl sulfoxide; TBA: tetra-*n*-butylammonium

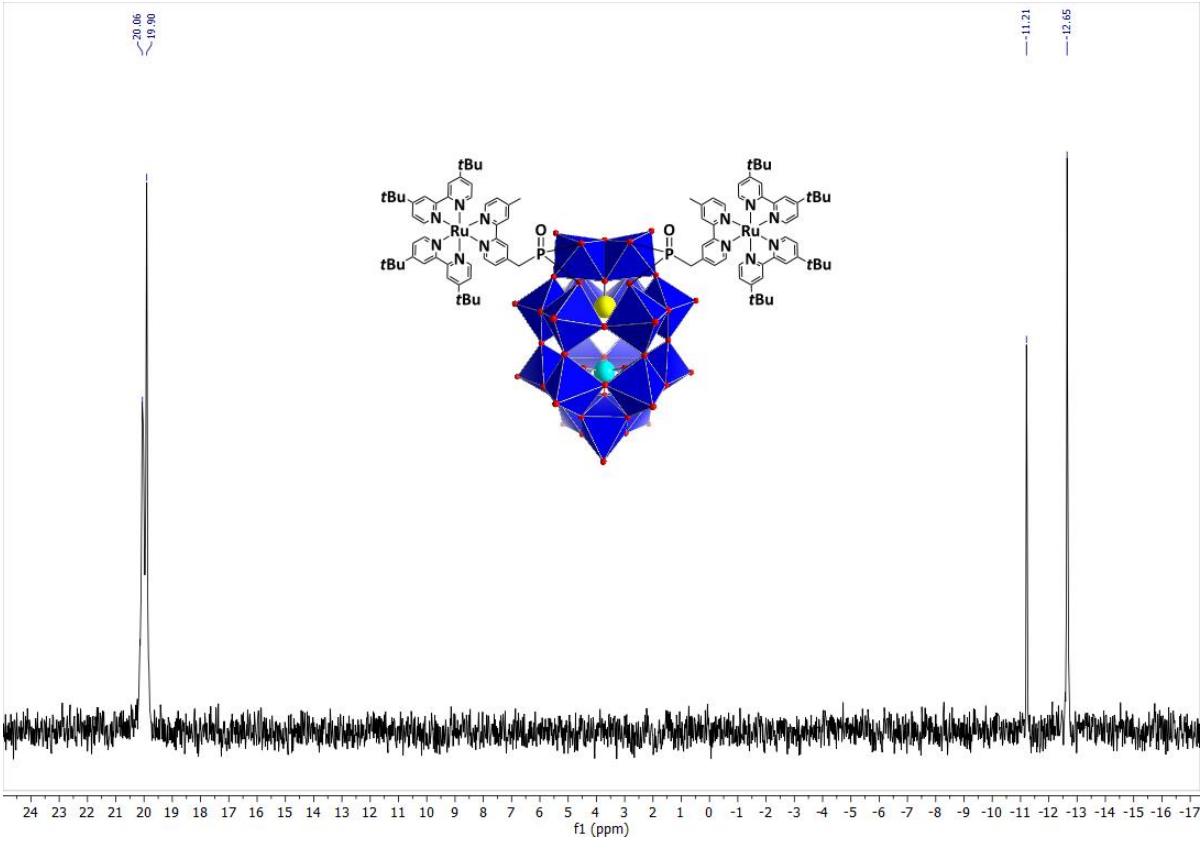

Figure 6: ^{31}P-NMR of **PS-POM** in DMSO-d_6 at r.t.

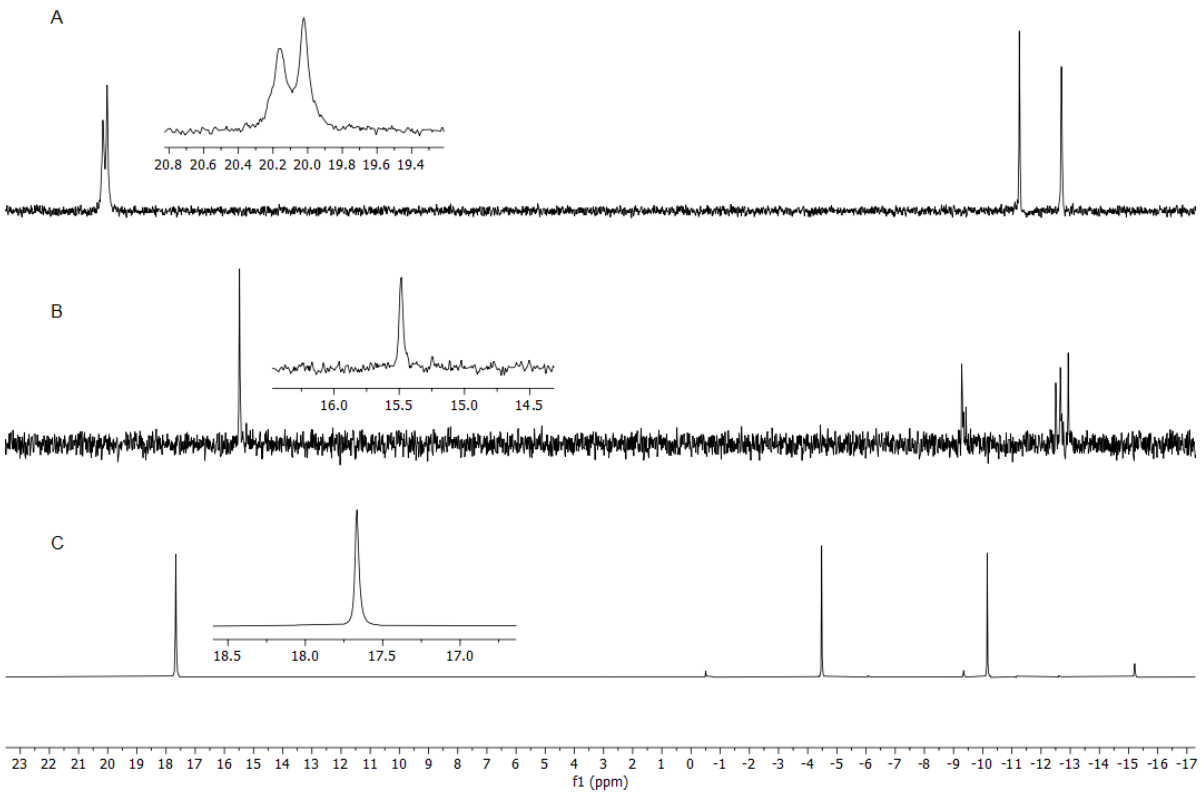

Figure 7: ^{31}P-NMR spectra of (A) **PS-POM**; (B) a mixture of the free phosphonic acid of **1** and **2;** (C) a mixture of **1** and **2** in DMSO-d_6 at r.t.

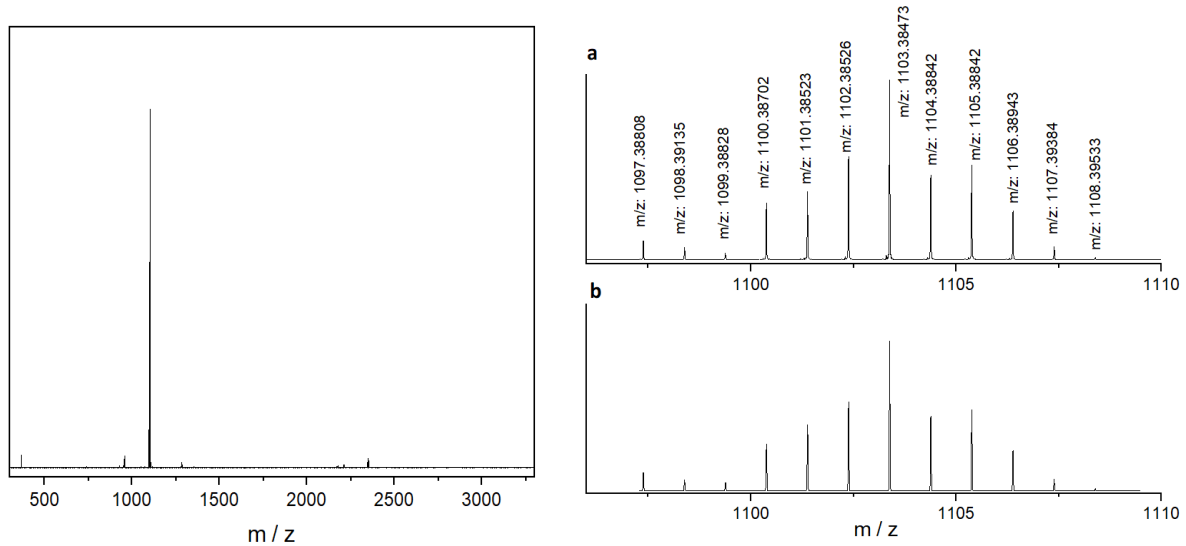

Figure 8: Left: MALDI Mass spectrometry of **1** in the 300 / 3000 m/z range. Right: high-resolution mass spectrum of the main peak of **1** (**a**) and simulated pattern (**b**).

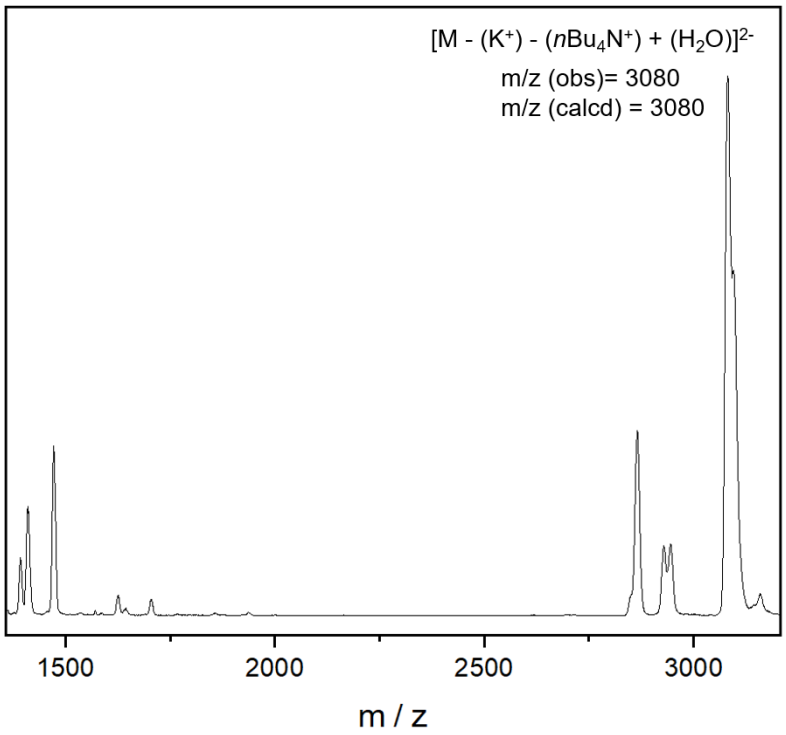

Figure 9: MALDI-TOF mass spectrometry of **PS-POM** in the 1300 – 3000 m/z range.

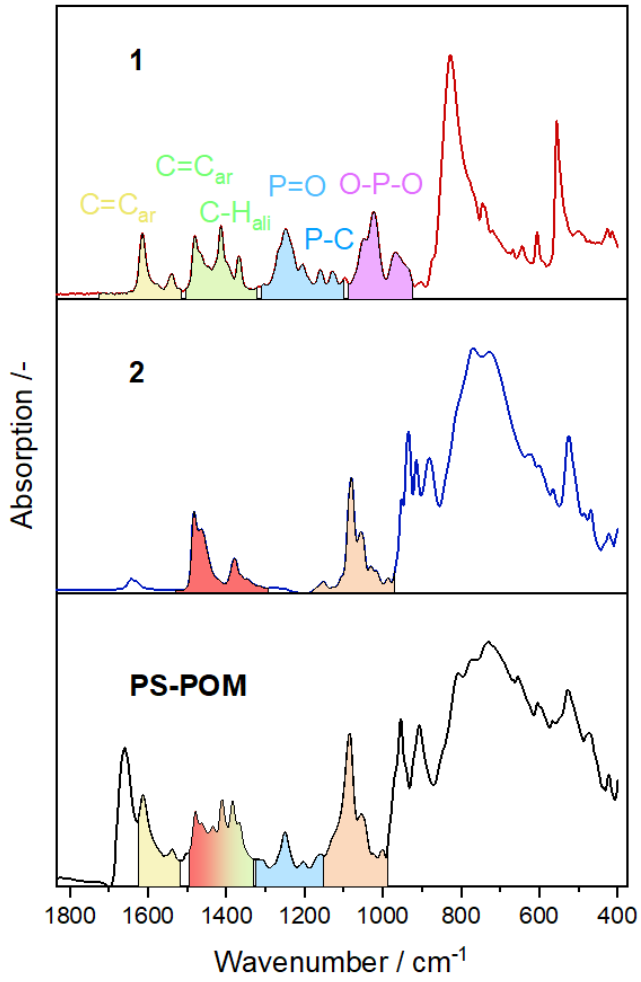

Figure 10: ATR-IR spectra of **1** (red), **2** (blue) and **PS-POM** (black).

3. Photoreduction experiments

All experiments were carried out in water-free, de-aerated DMF solution at the following concentrations: [**1**] = 5.8 µM, [**2**] = 2.9 µM, [**PS-POM**] = 2.9 µM, unless stated otherwise. The stock solutions were prepared under air and degassed with Argon (1 min per mL) and kept in an Argon-filled glovebox. Stock solution aliquots were transferred into gas-tight quartz glass cuvettes (d = 10.0 mm, Hellma). The samples were irradiated using 470 nm LEDs (*P* ca. 40 - 50 mW/cm^2) integrated in a custom-built reactor cooled by four fans, to maintain room temperature during irradiation.

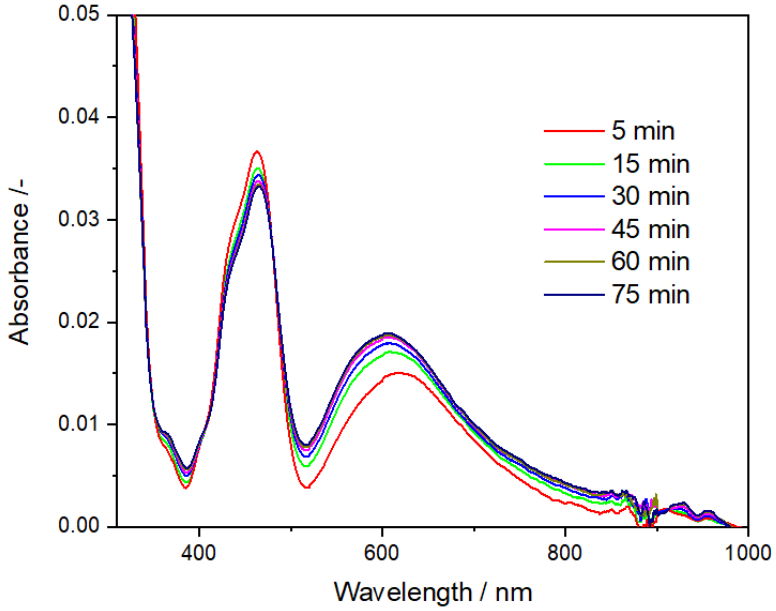

Figure 11: Time-dependent photoreduction of **PS-POM** with the electron donor triethylamine (TEA) (20 mM, 7000 eq.), $\lambda_{irradiation}$ = 470 nm, *T* = 25 °C, solvent: water-free, de-aerated DMF.

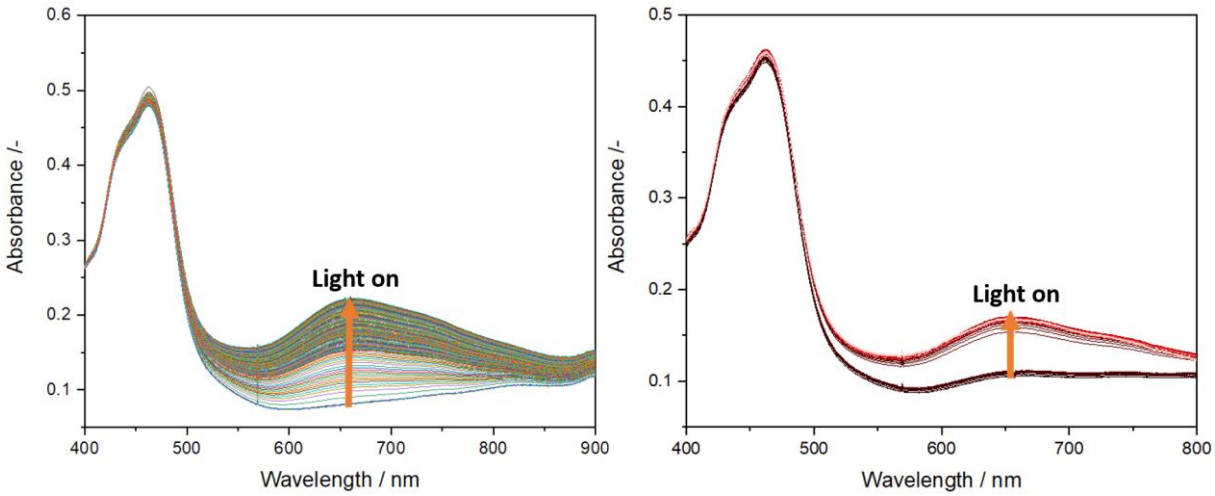

Figure 12: Left: time-dependent photoreduction of **PS-POM** using the sacrificial electron donor TEOA (60 mM, 6700 eq.). Right: time-dependent photoreduction of **PS-POM** in the presence of the electron donor Asc (6.5 mM, 720 eq.). Conditions: [**PS-POM**] = 9 µM; $\lambda_{irradiation}$ = 470 nm, *T* = 25 °C, $t_{irradiation}$ = 8 min; solvent: water-free, de-aerated DMF.

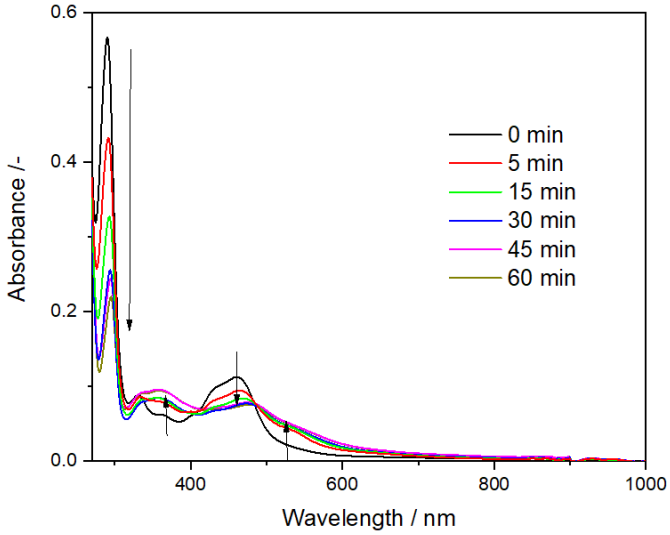

Figure 13: Time-dependent photoreduction of **1** with the electron donor TEA (20 mM, 3500 eq.), $\lambda_{irradiation}$ = 470 nm, *T* = 25 °C, solvent: water-free, de-aerated DMF.

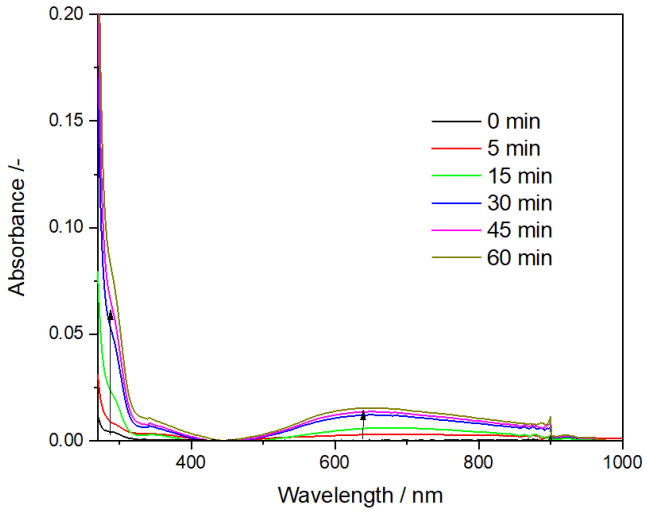

Figure 14: Time-dependent photoreduction of **2** using the electron donor TEA (20 mM, 7000 eq.), $\lambda_{irradiation}$ = 470 nm, *T* = 25 °C, solvent: water-free, de-aerated DMF.

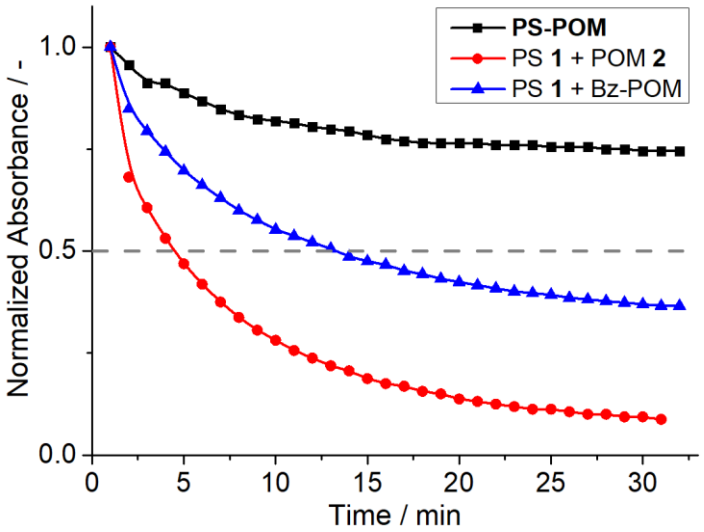

Figure 15: Time-dependent, normalized IVCT absorbance (recorded at 650 nm) of photochemically reduced solutions of **PS-POM**, and the references PS **1** / POM **2** and PS **1** / **Bz-POM** under dark conditions. For **PS-POM**, this experiment gave a $t_{1/2}$ of the reduced state of > 24 h. Conditions: water-free de-aerated DMF solutions, [**PS-POM**]: 18 µM, [**1**]: 36 µM, [**2**]: 18 µM, [**Bz-POM**]: 18 µM, electron donor: Asc (6.5 mM).

4. Electrochemistry

Electrochemical analyses were carried out in water-free, de-aerated DMF solutions (containing 0.1 M (nBu$_4$N)PF$_6$) under Argon atmosphere. Fc$^+$/Fc was used as internal reference. The prepared solutions of **PS-POM**, **1**, or **2** (*ca.* 2 mM) were degassed with Argon before use. Scan rate: 200 mV / s if not stated otherwise.

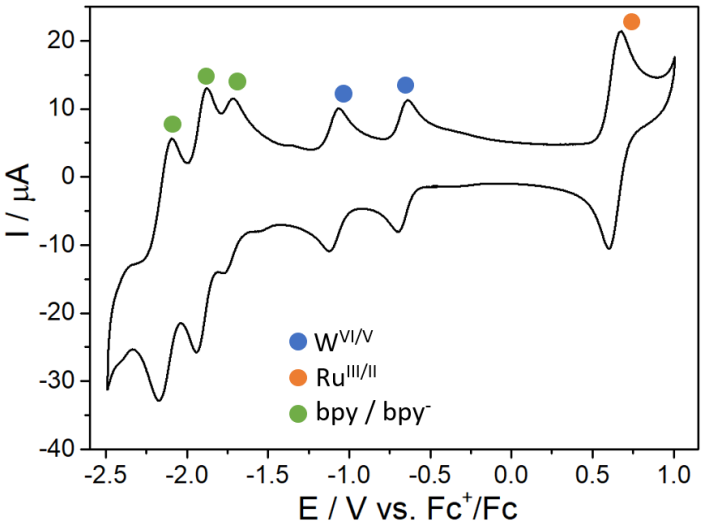

Figure 16: Cyclic voltammetry of **PS-POM** in water-free, de-aerated DMF solution (containing 0.1 M (nBu$_4$N)PF$_6$ as supporting electrolyte), scan rate = 200 mV / s.

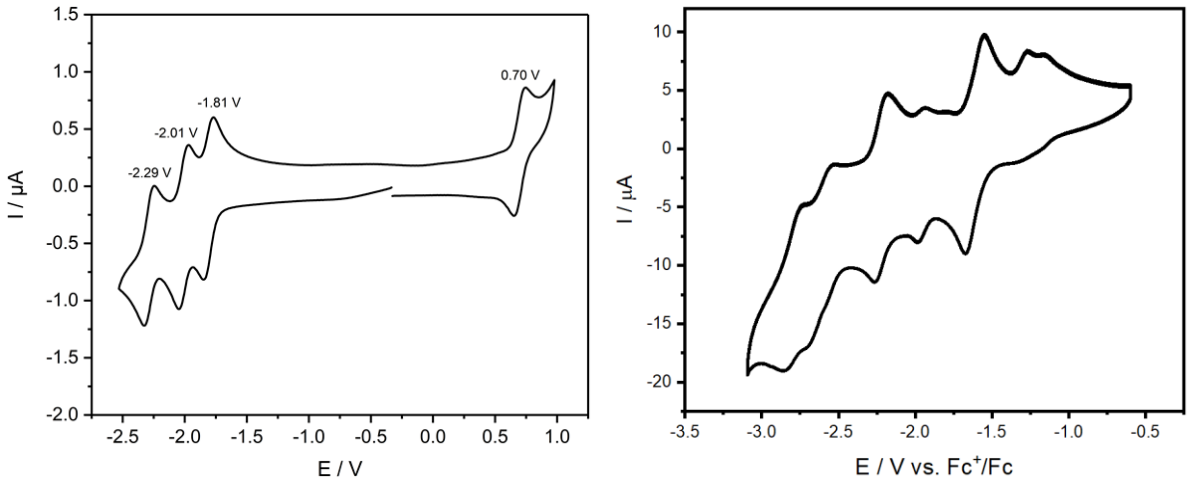

Figure 17: Left: cyclic voltammetry of PS **1**. **Right:** cyclic voltammetry of POM **2**. Conditions: solvent: DMF (containing 0.1 M (nBu$_4$N)PF$_6$), scan rate = 200 mV / s.

Table **S1**: Summary of electrochemical data obtained for **PS-POM**, **2** and **1**.

	Ru^{III}/Ru^{II}	$W_{(1)}{}^{VI}/W_{(1)}{}^{V}$	$W_{(2)}{}^{VI}/W_{(2)}{}^{V}$	$bpy_{(1)}/bpy_{(1)}{}^{\cdot-}$	$bpy_{(2)}/bpy_{(2)}{}^{\cdot-}$	$bpy_{(3)}/bpy_{(3)}{}^{\cdot-}$
PS-POM	0.63	-0.68	-1.10	-1.74	-1.90	-2.15
2	-	-1.32	-1.70		-	-
1	0.70	-	-	-1.81	-2.01	-2.29

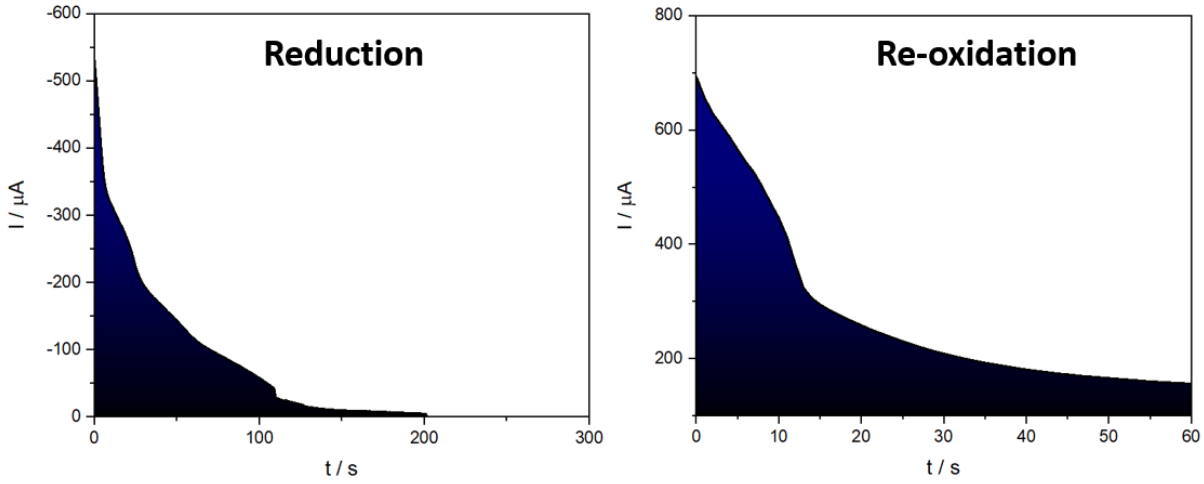

Figure 18: Chronoamperometry of the electrochemical reduction (**left**) and re-oxidation (**right**) of **PS-POM.** Conditions: water-free, de-aerated DMF solution. Reduction: $E_{reduction}$ = -1.37 V *vs*. Fc^+/Fc. Number of stored electrons per **PS-POM** molecule: 2.0. $E_{re\text{-}oxidation}$ = -0.2 V *vs*. Fc^+/Fc. Number of released electrons per **PS-POM** molecule: 1.8.

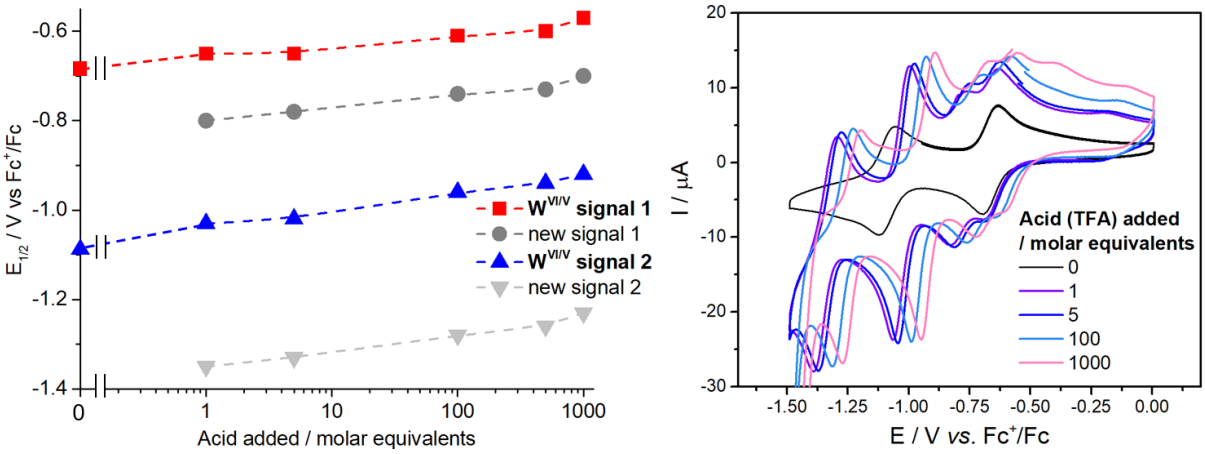

Figure 19: Left: changes in redox-potentials of the $W^{VI/V}$ redox-processes in **PS-POM** depending on the amount of trifluoroacetic acid (TFA) present. **Right:** corresponding cyclic voltammograms. Conditions: water-free, de-aerated DMF solution, [TFA] = 0 – 1000 equivalents relative to **PS-POM**. Note that the appearance of two new redox processes in the window studied could be due to the presence of different protonation states of **PS-POM**,[11,12] or ion-pairing effects with the nBu$_4$N$^+$ cations.[13] Experimental and theoretical studies are underway to gain more insights into this observation.

5. Spectro-electrochemistry

Spectro-electrochemistry was performed using a **PS-POM** solution in DMF (0.1 mM) under an Argon atmosphere. The solutions were thoroughly purged with argon before each measurement. The concentration of analyte and supporting electrolyte was the same as in the cyclic voltammetry measurements, unless stated otherwise. The reduction potentials used for the spectro-electrochemistry measurement were selected based on the CV data for **PS-POM**. The spectrum obtained for **PS-POM** was compared to the spectrum of **2** and confirmed that reduction occurs on the POM metal oxo framework.

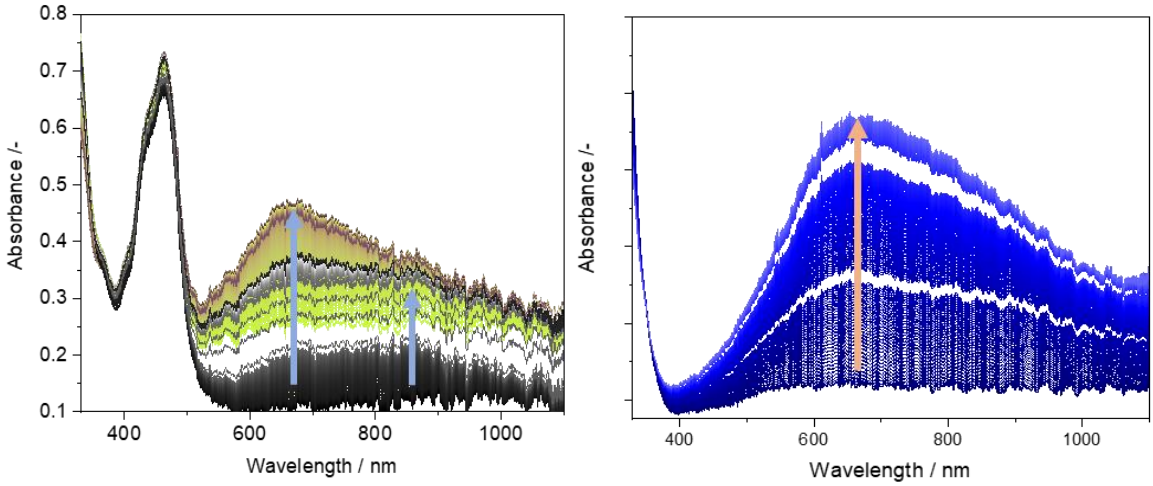

Figure 20: Left: spectro-electrochemistry of **PS-POM** in water-free, de-aerated DMF solution ([**PS-POM**] = 0.1 mM) at potentials of -0.8 V (black) and -1.1 V (green) *vs.* Fc^+/Fc. **Right:** spectro-electrochemistry of POM **2** in water-free, de-aerated DMF solution ([**2**] = 0.3 mM) at a potential of -1.87 V *vs.* Fc^+/Fc.

6. Time-resolved spectroscopy

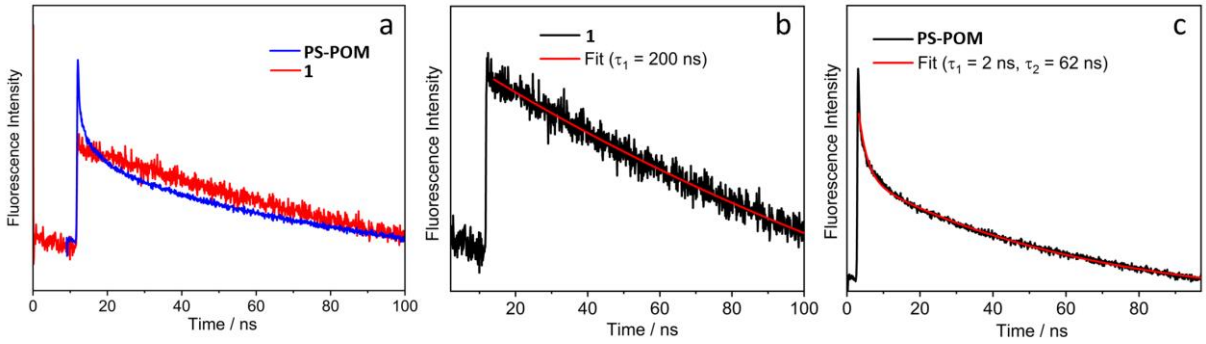

Figure 21 (a) emission decay profiles of **1** (red) and **PS-POM** (blue), measured by time-correlated single photon counting in DMF excited at 470 nm; (b) emission decay profile and exponential fit of **1**; (c) emission decay profile and exponential fit of **PS-POM.** The fitted emission lifetimes for **1** and **PS-POM** are given in the graphs.

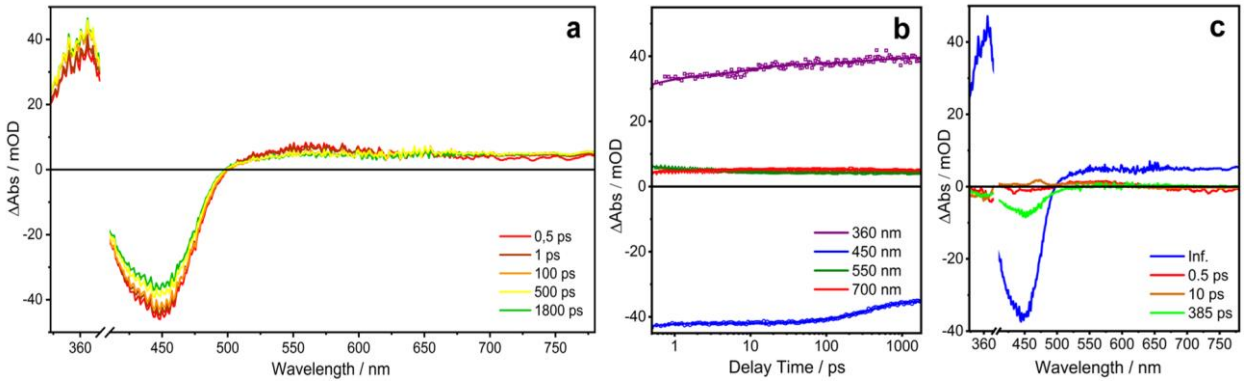

Figure 22: (a) transient absorption spectra of **1** at selected delay times; (b) transient kinetics at key wavelengths; (c) spectral changes associated with each kinetic process (decay-associated spectra - DAS) for **1** (in DMF), pumped at 400 nm.

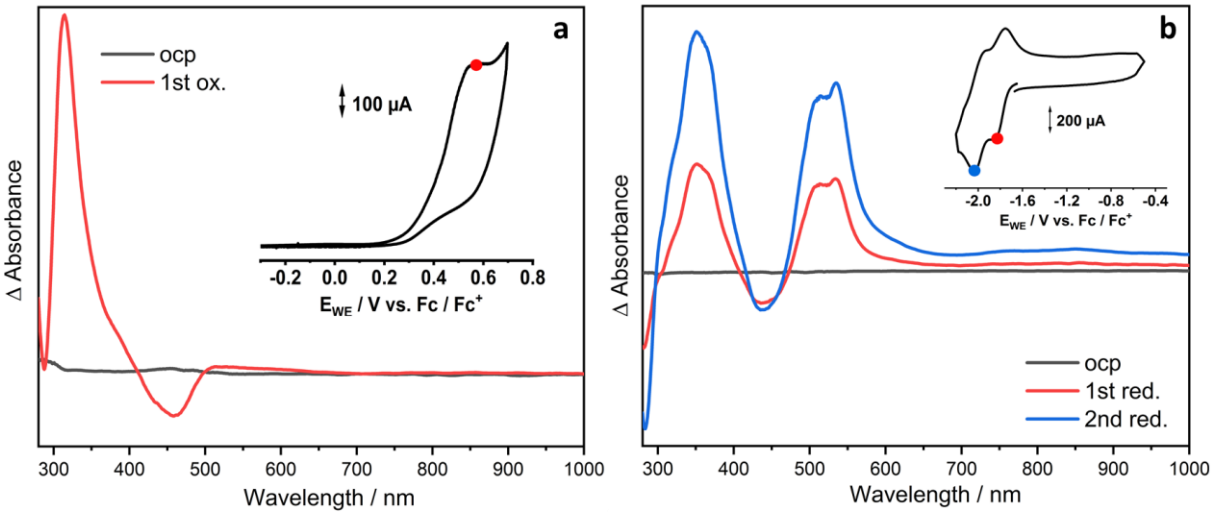

Figure 23: Differential UV-Vis spectroelectrochemical experiments of **1,** showing changes during the 1st oxidation (a) as well as the 1st and 2nd reduction (b) of **1**. Insets: CVs of **1** in 0.1 M (nBu$_4$N)BF$_4$ DMF solution, referenced against Fc$^+$/Fc. The applied potentials for acquisition of the differential UV-vis spectra are marked with red and blue dots (scan rate 100 mV/s, electrodes: working: glassy carbon, counter: Pt, pseudo-reference: Ag/AgCl).

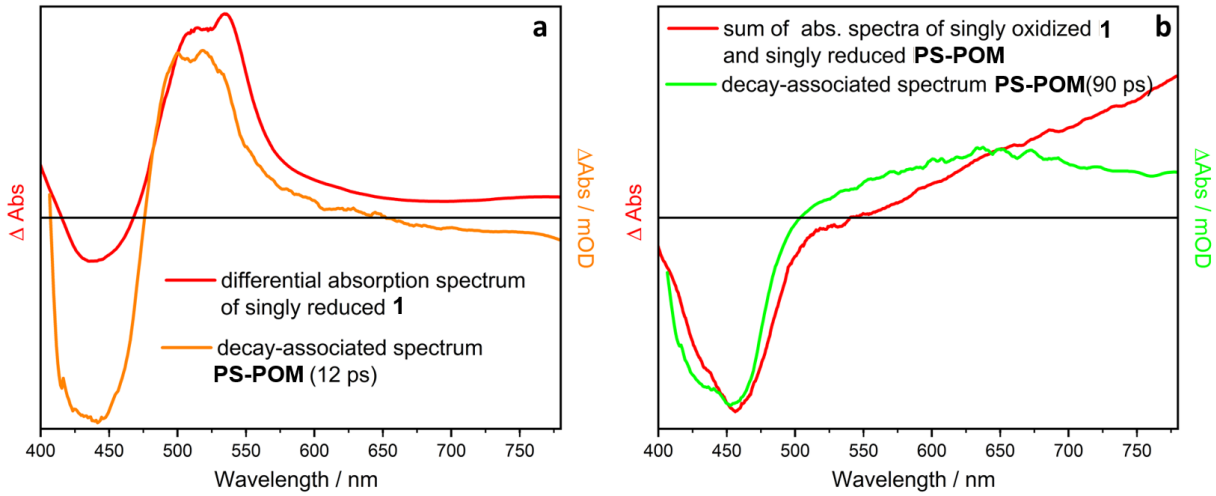

Figure 24: (a) Comparison of the second decay-associated spectra (DAS) of **PS-POM**, τ = 12 ps (also see Figure 4c, this 12 ps component reflects the decay of an intermediate of charge separation in which the bpy is reduced) with the differential UV-Vis spectroelectrochemical absorption spectra of singly reduced **1**. (b) Comparison of the third DAS τ = 90 ps of **PS-POM** (Fig. 4c, this 90 ps component reflects the decay of the charge-separated state) with the simulated sum of the differential UV-Vis spectroelectrochemical absorption spectra of singly oxidized PS and singly reduced **PS-POM**. The UV-Vis spectroelectrochemical results are scaled arbitrarily.

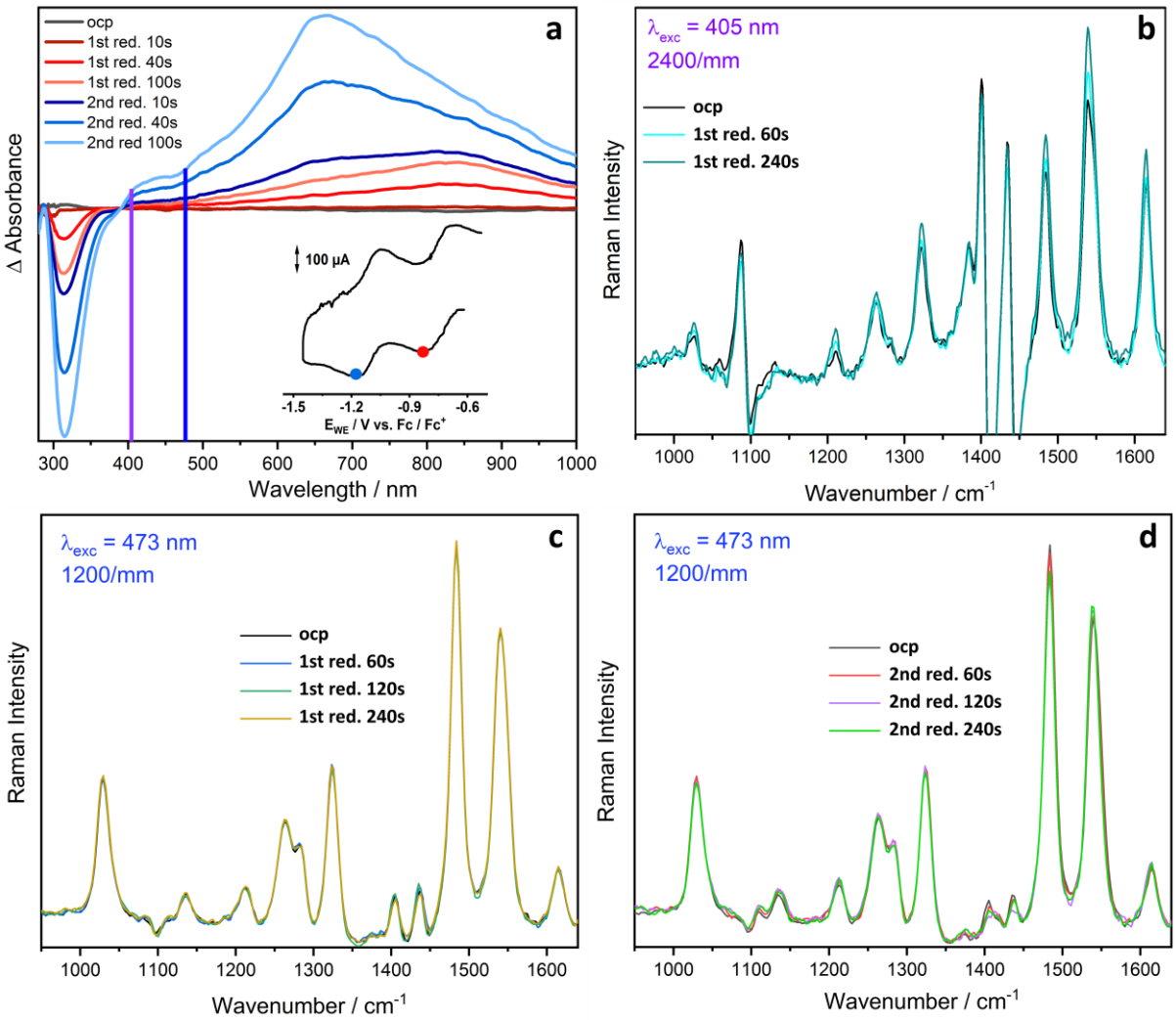

Figure 25: (a) Differential UV-Vis spectroelectrochemical experiments of **PS-POM**, showing changes during the 1st (red) and 2nd (blue) reduction of **PS-POM**. The rR excitation laser lines at 405 nm and 473 nm are displayed as vertical lines. Inset in (a): CV of **PS-POM** in 0.1 M ($nBu_4N)BF_4$ DMF solution, referenced against Fc^+/Fc. (b) – (d) experimental rR spectrum of **PS-POM** (black) and its reduction states, excited at 405 nm (b) and 473 nm (c, d). The region between 1400 and 1460 cm^{-1} in Panel b contains artifacts resulting from subtracting the solvent spectrum. Reduction of the POM fragment in **PS-POM** causes only minor changes in the rR spectra and therefore does not impact the chromophore properties of the Ru-photosensitizer components.

7. Energy diagram development

The energy diagram shown in the main manuscript, Figure 6b was established as follows:
(a) electrochemical potentials (*vs* Fc^+/Fc) were converted to eV (*vs* vacuum energy) using the relation *E*(in eV) = *E*(*vs* Fc^+/Fc, in eV) + 4.8 eV.[14]
(b) Redox potentials of the relevant species are taken from the corresponding electrochemical data in Table S1. Note that proton-free conditions were chosen (see Figure S19), as the exact mechanism of hydrogen evolution (*e.g.* whether protonated **PS-POM**-intermediates are involved is currently not known).[12]
(c) Under the given experimental conditions, the H^+/H_2 redox couple is located at 0.5 eV.[15]

8. HER Catalysis

Hydrogen evolution experiments were conducted using Schlenk tubes (borosilicate glass, V *ca*. 21 mL) sealed by a rubber septum (VWR, natural rubber), which was exchanged after every measurement. For a standard experiment, **PS-POM** and sacrificial electron donor were dissolved under argon atmosphere in water-free, de-aerated DMF at concentrations given in

the manuscript. The **PS-POM** solution was irradiated (monochromatic LED, λ_{max} 470 nm) for the desired period of time. The **PS-POM** reduction state was monitored by UV-Vis-NIR spectroscopy as described in the manuscript. Hydrogen release is possible by addition of the proton donor sulfuric acid to the reaction vessel *via* a Hamilton syringe (500 µL, 4 M in DMF) and the mixture was allowed to react for 5 min in the dark. Subsequent headspace gas chromatography was used to quantify H_2 evolution. Exclusion experiments confirmed that no hydrogen is formed in the absence of **PS-POM**, light or sacrificial electron donor. No hydrogen was detected when photosensitizer **1** was irradiated in the presence of an electron donor.

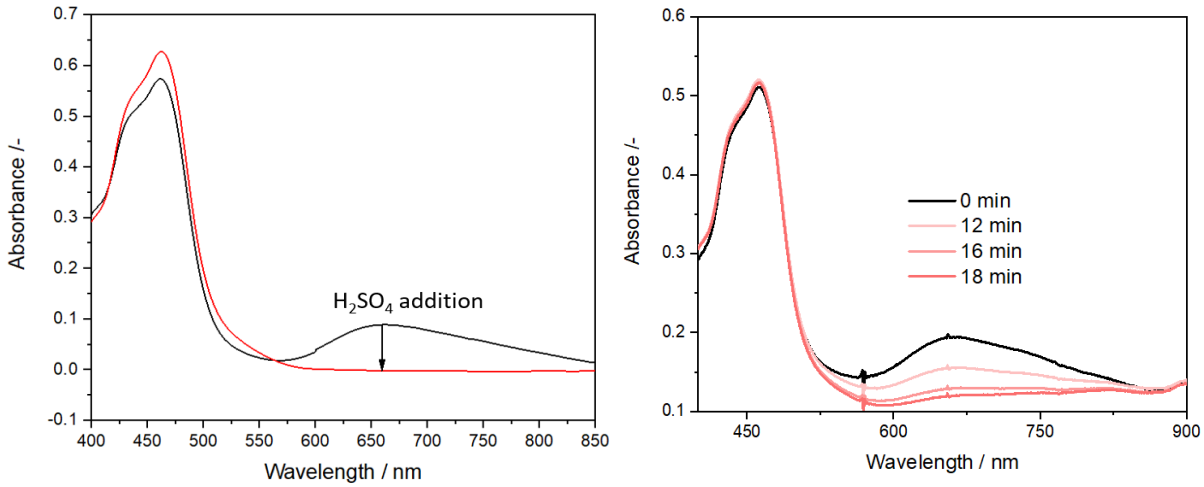

Figure 26: Left: UV-vis spectra of **PS-POM** (9 µM) with added sodium ascorbate (6.5 mM, 720 eq.) after irradiation for 15 min (black) and upon addition of H_2SO_4 (red). **Right:** UV-Vis spectroscopic reference experiment, showing the re-oxidation of **PS-POM** when exposed to atmospheric oxygen. Conditions: water-free, de-aerated DMF solution, [**PS-POM**] = 9 µM, sacrificial electron donor: TEOA (60 mM, 6700 eq.).

Table 2: summary of HER experiments performed with **PS-POM**.

$N_e^-/N_{PS\text{-}POM}$	$n_{PS\text{-}POM}$	n_{H2}	e^- to H_2 efficiency
1.96	150 nmol	60 nmol	41%

9. Crystallography

Suitable crystals of (mPO_3Et_2)bpy were obtained by slow evaporation of chloroform solution. (mPO_3Et_2)bpy crystallizes in the monoclinic space group $P2_1/c$ and does not differ from the corresponding symmetric analogs tetraethyl ([2,2'-bipyridine]-4,4'-diylbis(methylene))-bis(phosphonate) (bpyMeP) and 4,4´-dimethyl-2,2´-bipyridine with respect to the length of the central C6-C7 bond (ca. 1.49 Å) connecting the two pyridine spheres.[16,17] Additionally, very similar values for the central C5-C6-C7 angle and the central N1-C6-C7 angle compared with bpyMeP and 4,4´-dimethyl-2,2´-bipyridine were found. CCDC 2045447 contains the supplementary crystallographic data for this paper. These data can be obtained free of charge from The Cambridge Crystallographic Data Centre via www.ccdc.cam.ac.uk/structures.

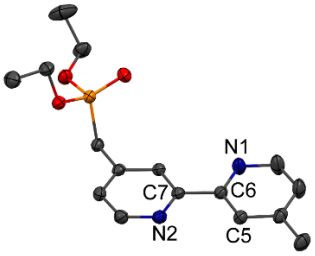

Figure 27: Solid-state structure of **(mPO_3Et_2)bpy**. The ORTEP ellipsoids are drawn at the 50% probability level and hydrogen atoms were omitted for clarity.

Table 3: Crystal data and structure refinement for (mPO_3Et_2)bpy.

CCDC no	2045447
Empirical formula	$C_{16}H_{21}N_2O_3P$
Formula weight	320.32
Temperature/K	150
Crystal system	monoclinic
Space group	$P2_1/c$
a/Å	11.7387(7)
b/Å	7.3238(4)
c/Å	19.4777(10)
α/°	90
β/°	95.087(2)
γ/°	90
Volume/Å^3	1667.94(16)
Z	4
ρ_{calc}g/cm^3	1.276
μ/mm^{-1}	0.178
F(000)	680.0
2Θ range for data collection/°	4.198 to 55.92
Index ranges	-15 ≤ h ≤ 15, -9 ≤ k ≤ 9, -25 ≤ l ≤ 23
Reflections collected	34593
Independent reflections	4000 [R_{int} = 0.0888, R_{sigma} = 0.0458]
Data/restraints/parameters	4000/0/202
Goodness-of-fit on F^2	1.061
Final R indexes [I>=2σ (I)]	R_1 = 0.0428, wR_2 = 0.1039
Final R indexes [all data]	R_1 = 0.0615, wR_2 = 0.1200
Largest diff. peak/hole / e Å^{-3}	0.49/-0.29

10. Quantum yield (QY) calculations

A literature-reported setup was used to determine the quantum yield of the PS-POM reduction.[9] DMF solutions of **PS-POM** (9 μM) were irradiated in the setup (LED, ($\lambda_{irradiation}$ = 470 nm) to determine P_{sample}. As reference, a cuvette containing only DMF was used to determine P_{ref}. P_{abs} was then calculated according to eq. 1, where *f* is a correction factor which corrects for the different distances of sample and detector to the light source. The **PS-POM** concentration was calculated based on the known molar absorption coefficients of the reduced species see above. Light power data were converted using the *Coherent PowerMax* software package. Quantum yields were calculated using eq. 2, where c_{prod} is the concentration of the reduced species, N_A is Avogadro's constant, h is Planck's constant, c is the speed of light, Δt is the time of irradiation and λ is the irradiation wavelength. Every measurement was conducted twice, and the average value is given in the manuscript.

$$P_{abs} = \left(P_{ref} - P_{sample}\right) \cdot f \qquad \text{eq. 1}$$

$$QY = \frac{c_{prod} \cdot V \cdot N_A \cdot h \cdot c}{P_{abs} \cdot \Delta t \cdot \lambda} \qquad \text{eq. 2}$$

11. Author contributions

S.A., S.K., A.K. M., S.R., B.D. and C.S. conceived the experiments and performed data analyses. S.A. and S.K. performed syntheses and characterization. S.A. and M.H. performed catalytic tests. C.L., L.Z. and B.D. performed time-resolved spectroscopy and provided data interpretation. D.N. and M.A. performed electrochemistry. W.T. and U.S.S. provided mass spectrometric data. A.K.M. performed crystallography. All authors co-wrote the manuscript.

12. References

1. Rau, S. *et al.* Bis(R-bipyridyl)ruthenium bibenzimidazole complexes (R = H, Me or But): supramolecular arrangement via hydrogen bonds, photo- and electro-chemical properties and reactivity towards carbon dioxide. *J. Chem. Soc. Dalt. Trans.* 3649–3657 (2000) doi:10.1039/b003992f.
2. Contant, R. *Inorganic Syntheses*. *Inorganic Syntheses* vol. 27 (1990).
3. Zedler, L. *et al.* Unraveling the Light-Activated Reaction Mechanism in a Catalytically Competent Key Intermediate of a Multifunctional Molecular Catalyst for Artificial Photosynthesis. *Angew. Chem. Int. Ed.* **58**, 13140–13148 (2019).
4. Siebert, R. *et al.* Spectroscopic Investigation of the Ultrafast Photoinduced Dynamics in π-Conjugated Terpyridines. *ChemPhysChem* **10**, 910–919 (2009).
5. Dobryakov, A. L., Kovalenko, S. A. & Ernsting, N. P. Coherent and sequential contributions to femtosecond transient absorption spectra of a rhodamine dye in solution. *J. Chem. Phys.* **123**, 044502 (2005).
6. Sheldrick, G. M. A short history of SHELX. *Acta Crystallogr. Sect. A Found. Crystallogr.* **64**, 112–122 (2007).
7. Sheldrick, G. M. Crystal structure refinement with SHELXL. *Acta Crystallogr. Sect. C Struct. Chem.* **71**, 3–8 (2015).
8. Macrae, C. F. *et al.* Mercury: Visualization and analysis of crystal structures. *J. Appl. Crystallogr.* **39**, 453–457 (2006).
9. Megerle, U., Lechner, R., König, B. & Riedle, E. Laboratory apparatus for the accurate, facile and rapid determination of visible light photoreaction quantum yields. *Photochem. Photobiol. Sci.* **9**, 1400–1406 (2010).
10. Kodama, K., Kobayashi, A. & Hirose, T. Synthesis and spectral properties of ruthenium (II) complexes based on 2 , 2 0 -bipyridines modified by a perylene chromophore. *Tetrahedron Lett.* **54**, 5514–5517 (2013).
11. Nambu, J., Ueda, T., Guo, S.-X., Boas, J. F. & Bond, A. M. Detailed voltammetric and EPR study of protonation reactions accompanying the one-electron reduction of Keggin-type polyoxometalates, [XVVM11O40]4− (X = P, As; M = Mo, W) in acetonitrile. *Dalton Trans.* **39**, 7364 (2010).
12. Prenzler, P. D., Boskovic, C., Bond, A. M. & Wedd, A. G. Coupled Electron- and Proton-Transfer Processes in the Reduction of α-[P 2 W 18 O 62] 6 - and α-[H 2 W 12 O 40] 6 - As Revealed by Simulation of Cyclic Voltammograms. *Anal. Chem.* **71**, 3650–3656 (1999).
13. Rahman, M. A., Gundry, L., Ueda, T., Bond, A. M. & Zhang, J. Electrode Material Dependence, Ion Pairing, and Progressive Increase in Complexity of the α-[S 2 W 18 O 62] 4–/5–/6–/7–/8–/9–/10– Reduction Processes in Acetonitrile Containing [n -Bu 4 N][PF 6] as the Supporting Electrolyte. *J. Phys. Chem. C* **124**, 16032–16047 (2020).
14. Tang, M. L., Reichardt, A. D., Wei, P. & Bao, Z. Correlating Carrier Type with Frontier Molecular Orbital Energy Levels in Organic Thin Film Transistors of Functionalized Acene Derivatives. *J. Am. Chem. Soc.* **131**, 5264–5273 (2009).
15. Pegis, M. L. *et al.* Standard Reduction Potentials for Oxygen and Carbon Dioxide Couples in Acetonitrile and N , N -Dimethylformamide. *Inorg. Chem.* **54**, 11883–11888 (2015).
16. Pearson, P. *et al.* Carbonyl−Carboxylato−Ruthenium Complexes Incorporating Diimine Ligands and Unexpected Cyclometalation of Carboxylate Ligands. *Inorg. Chem.* **43**, 683–691 (2004).
17. Braumüller, M. *et al.* Synthesis and characterization of an immobilizable photochemical molecular device for H 2 -generation. *Dalton Trans.* **44**, 5577–5586 (2015).